

Article

The Impact of Meteorological and Hydrological Memory on Compound Peak Flows in the Rhine River Basin

Sonu Khanal ^{1,2,*}, Arthur F. Lutz ¹, Walter W. Immerzeel ⁴, Hylke de Vries ³,
Niko Wanders ⁴ and Bart van den Hurk ^{2,3}

¹ FutureWater, Costerweg 1V, 6702 AA Wageningen, the Netherlands; a.lutz@futurewater.nl

² Vrije Universiteit Amsterdam, De Boelelaan 1105, 1081 HV Amsterdam, The Netherlands; hurkvd@knmi.nl

³ KNMI—Royal Netherlands Meteorological Institute, 3731 GA De Bilt, The Netherlands;
hylke.de.vries@knmi.nl

⁴ Department of Physical Geography, Utrecht University, 3508 TC Utrecht, The Netherlands;
W.W.Immerzeel@uu.nl (W.W.I.); N.Wanders@uu.nl (N.W.)

* Correspondence: s.khanal@futurewater.nl

Received: 19 February 2019; Accepted: 23 March 2019; Published: 31 March 2019



Abstract: Spatio-temporal variation of hydrological processes that have a strong lagged autocorrelation (memory), such as soil moisture, snow accumulation and the antecedent hydro-climatic conditions, significantly impact the peaks of flood waves. Ignoring these memory processes leads to biased estimates of floods and high river levels that are sensitive to the occurrence of these compounding hydro-meteorological processes. Here, we investigate the role of memory in hydrological and meteorological systems at different temporal scales for the Rhine basin. We simulate the hydrological regime of the Rhine river basin using a distributed hydrological model (SPHY) forced with 1950–2000 atmospheric conditions from an ensemble simulation with a high resolution (0.11°/12 km) regional climate model (RACMO2). The findings show that meltwater from antecedent anomalous snowfall results in a time shift of the discharge peak. Soil moisture modulates the rainfall-runoff relationship and generates a strong runoff response at high soil moisture levels and buffers the generation of runoff peaks at low levels. Additionally, our results show that meteorological autocorrelation (manifesting itself by the occurrence of clustered precipitation events) has a strong impact on the magnitude of peak discharge. Removing meteorological autocorrelation at time scales longer than five days reduces peak discharge by 80% relative to the reference climate. At time scales longer than 30 days this meteorological autocorrelation loses its significant role in generating high discharge levels.

Keywords: memory; auto correlation; compound events

1. Introduction

In many natural systems memory effects play a prominent role. Although the memory of atmospheric processes generally does not entail more than a few days [1–4], atmospheric autocorrelation is propagated to the slow hydrological storage reservoirs such as soil moisture (hereafter referred to as SM), snow pack, glaciers, groundwater and riverine storage [5,6]. Hydrologic processes with longer time scales “remember” past atmospheric anomalies and their effects are reflected in subsequent events or periods. For instance, a storm event may persist within the soil columns for a long time even after the external forcing has ceased. Similarly, accumulation of heavy snowfall may persist for a long time ultimately affecting the hydrological regime of a region.

Hydrological systems are governed by processes with memory at different time scales [7]. Examples are evaporation [8,9], ground water [10,11], SM [1,12], snow dynamics [13–15] and riverine

storage [6] having memory of days to up to several years. Similarly, the long term persistence—or ‘Hurst phenomenon’—has triggered many studies supporting engineering applications such as design discharge for hydraulic infrastructure [16], lake inflows [17], river inflows [18], the regional hydrological cycle [19], floods [20] and droughts [21]. Predictability studies have addressed SM memory effects [22–24], ground water memory [10,11,25,26] and snow memory [15,27,28].

In reality, many phenomena act simultaneously, and their compound occurrence is highly influential in determining the final state of the system [29]. For instance, persistence in SM may lead to a drought during warm periods [1,30] but can similarly increase the likelihood of severe floods during cold periods [31,32]. Likewise, snowfall from a prior season can strongly modulate subsequent stream flow.

The co-occurrence of hydro-climatic extremes may propagate disproportionately to extreme hydrological events. For instance, the co-occurrence of heavy precipitation with heavy snowmelt, high SM or high groundwater levels can lead to extreme discharge. This compounding nature of extreme events may be crucial to understand the background of extreme hydrological events [33–37]. Hydrometeorological compound events (CEs) are increasingly receiving scientific attention [29,38,39]. This study primarily focuses on compound hydrometeorological events and their intensification by the memory of hydrological processes. For Dutch coastal areas, several studies describe CEs for storm surges in combination with wind [34], precipitation [33,34,38,40,41] and discharge [35,42]. These studies confirm a clear correlation structure among the compound occurrence of storm surges and discharge (precipitation). Further, they share some shortcomings emanating from using limited observation records, reanalysis products or model simulations, and/or focusing on a limited dynamic range of the lagged signals contributing to the CEs [33–35,40,41]. Moreover, these studies focused on a predefined timescale without explicitly exploring the role of process memory in the governing hydrometeorological systems. In a large river basin like the Rhine, where basin SM and snow storage in the Alps and upper Rhine play an important role in determining the flow regime, extreme antecedent rainfall or snowfall can contribute to elevated risk of high discharge, leading to coastal or fluvial flooding. A significant part of the precipitation during the winter months (DJF) is temporarily stored as snow in the upper/alpine part of the Rhine [42,43]. The stored snow releases the meltwater with a certain time delay [44], and contributes annually around 34% to the discharge at Lobith [45]. The co-occurrence of snowmelt either with a persistent single low depression or sequence of low depressions extending over multiple weeks can result in high discharge volumes [46]. Extreme rainfall on frozen or saturated soil can also generate extreme floods in the Rhine [47]. In addition, high discharge of the Rhine at Lobith requires a series of moisture laden low pressure depressions passing over the basin [48,49]. The most destructive floods in Netherlands in 1926 (heavy rainfall episodes leading to dike breach), 1993 (heavy rainfall episodes on saturated soil), and 1995 (rain on frozen soil) are examples of CEs. A good understanding of the memory processes and their nonlinear interaction with extremes is required to correctly estimate risk imposed by these CEs.

A deeper analysis for such CEs requires a consistent long spatial-temporal dataset for soil moisture, snowfall and snowmelt. There are no such datasets available for historical periods. It is a challenging task to analyze the CEs from a limited observed record [33]. Several studies have shown that long and realistic simulations of hydrodynamic processes and events can bypass the limitation posed by the limited observation record and improve the accuracy of estimation of the statistical properties of compound extreme events [33,34,41]. However, the climate data requires downscaling and bias correction of precipitation and temperature fields before it could be used for the hydrological impact studies [50–52].

In this study we synthesize to what extent memory within hydro-meteorological systems affects the generation of extreme discharge. We particularly investigate memory effects at monthly to seasonal timescales. To achieve this, first, we explore the role of meteorological autocorrelation by perturbing the time-correlation of the meteorological time series used as forcing for streamflow simulations by a hydrological and hydraulic model system. Next, we investigate the role of snow and SM memory in the

hydrological regime of the Rhine. Finally, we analyze the role of memory in the hydro-meteorological system that leads to intensification of the hydrological extremes.

2. Study Area

The Rhine basin covers an area of 185,000 km² and runs over 1320 km from its source in the Alps to the North Sea. The largest fraction of the basin (about 2/3rd) is located in Germany, amongst the nine countries through which the Rhine flows (Figure 1). Along its course, the Rhine collects water from major tributaries like the Aare, Neckar, Main and Moselle. The mean annual precipitation across the Rhine basin varies from about 500 (Rhine valley) to 2000 mm (Alpine region), and the mean annual discharge at Lobith is about 2200 m³s⁻¹. During summer the streamflow for the upper part of Rhine at Basel is dominated by snowmelt and rainfall-runoff from the Alps [53]. However, for the lower parts at Lobith, the Netherlands, streamflow is dominated by rainfall resulting in streamflow peaks during winter. The annual mean hydrograph shows a change of the discharge peak from summer to winter when descending from the upper Rhine at Basel down to the lower Rhine at Lobith [47,54]. The annual mean contribution of snowmelt to total streamflow at Lobith is around 34% [45], while discharge from the area upstream of Basel consists of snowmelt for almost 50% [55]. The travel time of the flood wave between Basel and Lobith is around five days [56]. Downstream of Lobith, the Netherlands is protected by numerous dikes measuring a total length about 22,000 km.

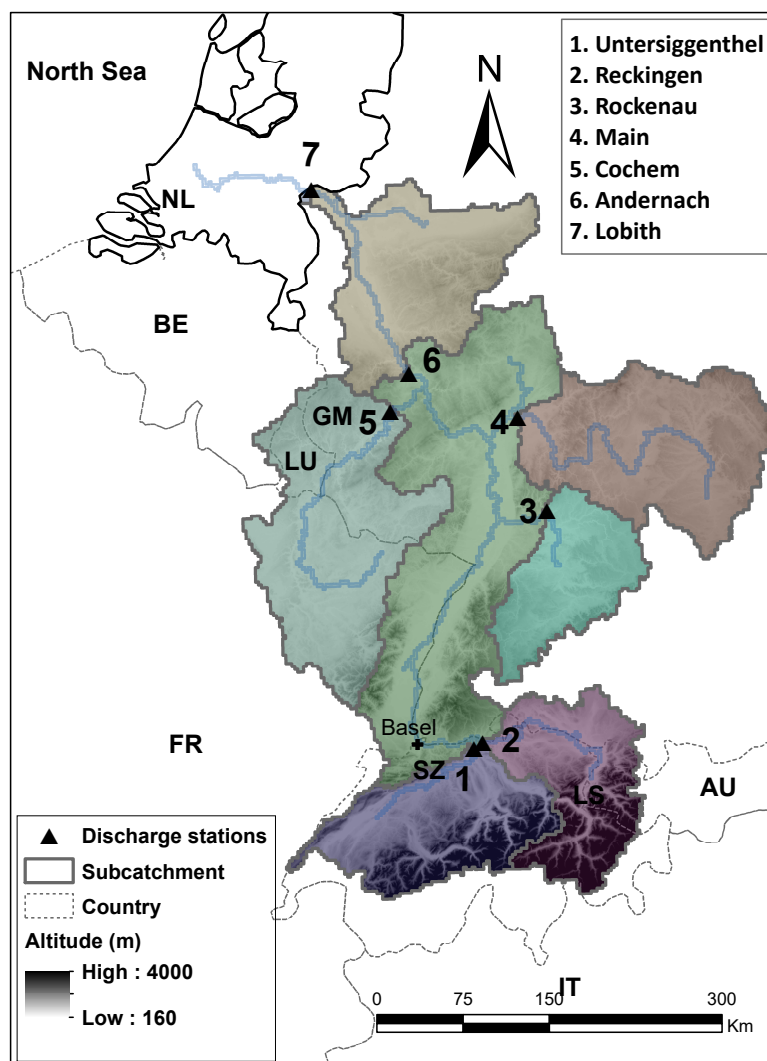


Figure 1. The Rhine basin, with seven sub catchments used for the calibration.

The highest discharge ever recorded in the Rhine at Lobith is about $12,000 \text{ m}^3 \text{ s}^{-1}$ during the floods of January 1926, which was primarily caused by multi-day episodes of rainfall after a period of moderate rain filling up the SM reservoir, in combination with melting of snow stored over the previous winter. Similarly, in December 1993 a flooding was caused by an extreme 10-day rainfall sum on saturated soil. In January 1995 an anomalous high temperature episode following a cold spell caused a coincidence of precipitation falling as rain on frozen soil and melting of snow leading to a strong discharge peak. Current protection levels for flood infrastructure in the Netherlands are designed to withstand a flood event of a strength that has a recurrence time of 1250 years [57]. This leads to a so-called “design discharge” of $16,000 \text{ m}^3 \text{ s}^{-1}$. Discussions to increase this level to higher discharge volumes, to account for changing climate and socio-economic conditions, are ongoing.

3. Data, Model and Methods

3.1. Data

In this study we used daily output from a 16-member ensemble of climate model simulations with the Global Climate Model (GCM) EC-Earth for the period 1951–2000 [58]. The 12 km resolution Regional Climate Model (RCM) RACMO2 was used to dynamically downscale the GCM ensemble [59]. E-OBS v14 daily gridded precipitation data at 0.25° resolution were used for the bias correction of outputs from the RCM [60]. Daily temperatures were adjusted to local topography using a vertical lapse rate of $-6.5 \text{ }^\circ\text{C km}^{-1}$. The downscaled data were used as input for the hydrological model.

3.2. Hydrological Model

In this study we used the Spatial Processes in Hydrology (SPHY) hydrological model [61]. SPHY is a conceptual, spatially distributed (raster-based) “leaky-bucket” type model. The model integrates dominant hydrological processes like (i) rainfall–runoff; (ii) lake/reservoir outflow, (iii) cryospheric processes (snow, ice, glaciers) (iv) evapotranspiration and (v) soil hydrological processes. SPHY requires input data as fixed state and dynamic variables. Digital Elevation Model (DEM), land use type, glacier cover, reservoirs and soil characteristics are the relevant fixed state variables. The main dynamic variables are meteorological data such as precipitation and temperature (maximum, minimum and average). The model contains sub-grid variability (e.g., cells can be glacier-free or partially to fully covered with glaciers) and melt generation is based on the widely used degree-day melt modeling approach [62]. The snow storage at each time step is updated with snow accumulation and/or snowmelt. Precipitation is segregated in the form of rain or snow, depending on the temperature. Precipitation can be intercepted by canopy and in part or in whole evaporated. The reference evapotranspiration is calculated using the modified Hargreaves method [63]. A fraction of the liquid precipitation contributes to the surface runoff, whereas the remainder infiltrates into the soil. The resulting soil moisture, depending on the soil properties and fractional vegetation cover, is available for the evapotranspiration, while the remainder contributes in the long-term to river discharge by means of lateral flow from the first soil layer, and base flow from the groundwater reservoir. Glacier ice melt contributes to the river discharge by means of a slow and fast component, being (i) percolation to the groundwater reservoir that eventually becomes base flow, and (ii) direct runoff. The cell specific sum from surface runoff, lateral flow, base flow, snowmelt and glacier melt is further routed. It is coupled to the PCRaster Global Water Balance model (PCR-GLOWB2) kinematic wave routing scheme to represent the hydrodynamic processes in the basin [64]. SPHY is calibrated and validated against observed daily discharge, obtained from the Global Runoff Data Centre, at seven locations (Figure 1) along the Rhine for the period of 1989–2000 [65]. The model is calibrated for the time period 1989–1995 and validated for 1996–2000. The calibration was done sequentially for five independent upstream locations and subsequently for the two downstream locations Andernach and Lobith. We used the mean square error (MSE) as the objective function and maximum likelihood estimation (MLE) to calibrate the model parameters [35]. The generated daily specific fluxes from

SPHY for each grid cell are then routed through the river network using the simple kinematic wave scheme from PCR-GLOBWB 2 model (hereafter referred to as 'routing model'). The routing model is calibrated for the Manning's n value using the observed discharge.

3.3. Snow Memory Effects

To investigate the effects of snow memory on the hydrological regime of the Rhine, we used a conditional sampling approach. From the 16 ensemble simulations we sampled hydrological years with above average and below average snowfall in separate bins, and assessed the discharge characteristics for the two sets of years. To account for snow accumulation and ablation the hydrological year runs from October until September in the next year.

3.4. Soil Moisture Memory Effects

Conditional sampling was also applied to study the impact of SM memory effects. The SM calculated is only confined to the top rootzone layer. The rootzone layer, a calibration parameter in SPHY model, varies from 50 (Alpine parts) to 500 mm (lower valley) along the basin. We used the fraction of actual water stored in the top rootzone layer and the potential capacity of rootzone layer to calculate the dimensionless SM. Winter and summer months which are preceded by a 10-day precipitation sum exceeding the long-term 95% percentile value are separately stored and analyzed. This selection reflects anomalously high initial SM values that limit the soil infiltration capacity for subsequent rainfall events.

The interaction of PPT in combination with SM on discharge was assessed based on the multi-conditional sampling method. First, two groups of PPT samples, high (HPPT) and low (LPPT), were separated by above and below median 10-day cumulative PPT values. Then from each of PPT groups two sub groups, climatological and anomalously low (<10% quantile, LSM) and high (>90% quantile, HSM) initial (beginning of 10 day) SM, were segregated. We thus created four groups of 10-day samples, namely LPPT_LSM (low precipitation and low SM), LPPT_HSM (low precipitation and high SM), HPPT_LSM (high precipitation and low SM) and HPPT_HSM (high precipitation and high SM). Finally, we compared the discharge characteristics in each of these samples and evaluated the effect of antecedent SM conditions on discharge. While analyzing the data it was ensured that the SM and discharges were segregated at the beginning and end of the 10 days period of each event respectively.

3.5. Meteorological Autocorrelation

Meteorological autocorrelation results from the occurrence of clustered rainfall events, e.g., series of low depressions passing the Rhine basin. We tested the sensitivity of the occurrence of peak discharge in the Rhine basin to the length of the autocorrelation time scale of the sequence of daily weather events. The evaluation was carried out by removing autocorrelation at chosen time scales by reconstructing the meteorological time series using a randomized selection from the 800 years of model data. In this reconstruction, precipitation and temperature fields were selected jointly without replacement, retaining consistency between these meteorological variables, and the structure of the spatial patterns [66,67]. This is analogous to a non-parametric resampling weather generation method. The reshuffling procedure does preserve the probability density distribution of the original time series.

The shuffling was applied using five different time scales. All autocorrelation exceeding a daily time scale was removed by randomly resampling daily meteorological fields. Autocorrelation at the five-day time scale is retained by resampling five-day blocks of meteorological fields, thereby removing all autocorrelation beyond a five-day time scale. Similar procedures were applied to time scales of 10, 30 and 180 days. Figure 2 illustrates the procedure. These sets of weather sequences serve as input forcing for SPHY and the routing model.

Finally, in a set of specific case studies, we analyzed a number of synoptic meteorological patterns leading up to an extreme hydrological event. We selected two synoptic meteorological patterns that

lead to the generation of extreme discharge, one for the original and one for the shuffled simulations using one-day selection blocks. The comparison of these anecdotal situations provides insight in the role of memory in the meteorological systems for the generation of extreme discharge. We investigated the climatology and anomaly of mean sea level pressure (SLP), wind speed, precipitation, rainfall, SM and temperature corresponding to the extreme discharge for each of the two cases. We also investigated the role of compounding snow, rain and SM to generate the extreme discharge.

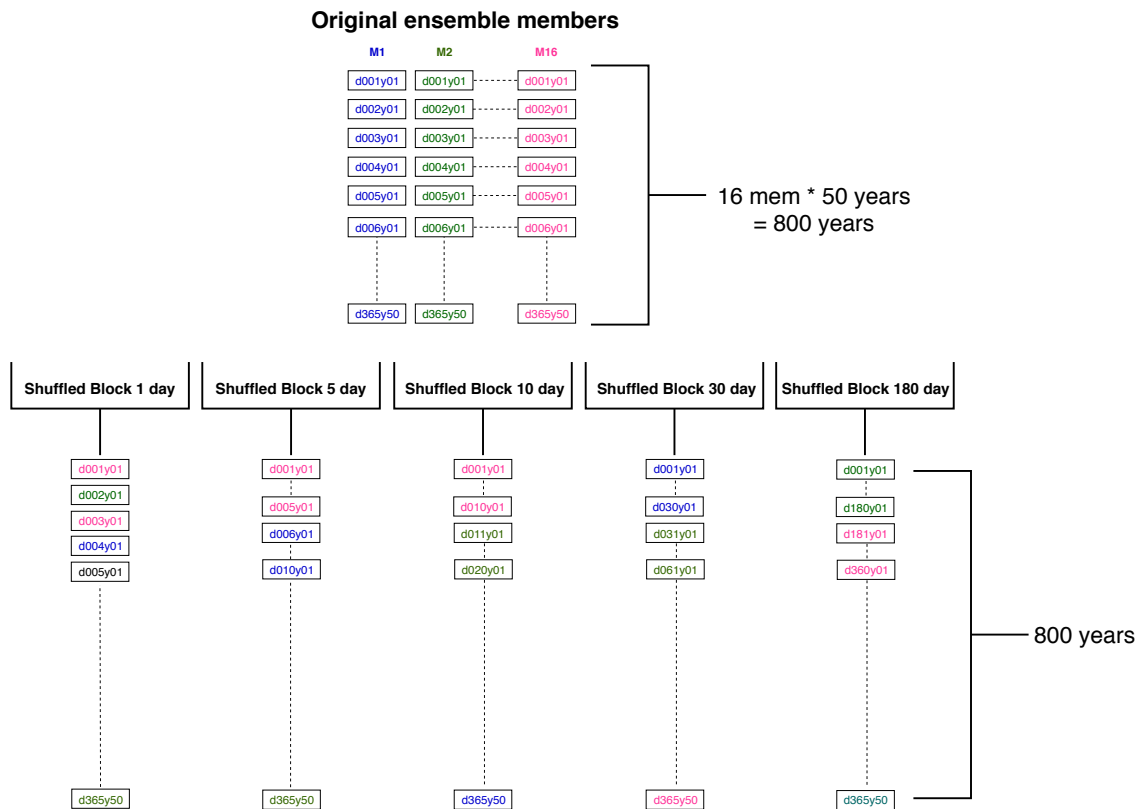


Figure 2. The resampling technique used in the study. ‘d’ stands for the calendar day, ‘y’ stand for the year and ‘M’ stands for the ensemble member number. The color designates the sequences of days kept together as per the block and data from the same ensemble member is used. For instance, in the block of five days, the five days memory is preserved both in temperature and precipitation. The block containing day one (d001) to day five (d005) has been taken from a given ensemble member (16). For the subsequent five day block (d006–d010) another ensemble member (01) is randomly chosen.

4. Results and Discussion

4.1. Performance of the Hydrological Model

We assessed the performance of the hydrological and routing model in two steps. First the daily flow at Lobith was compared to observations. Next, the temporal characteristics of the flood wave were assessed to check the ability of the model to generate realistic peak discharge features.

4.1.1. Daily Flows

First, we compared the simulated discharge at Lobith to the observed time series separately for the calibration and validation period as shown in Table 1 [65]. During the calibration period, the model simulates the observed discharge values fairly well, with an overall bias and Nash Sutcliffe Efficiency (NSE) of 3.3% and 0.78, respectively [68]. The 95th quantile of discharge is overestimated on average by 4.5%, which is acceptable given the fact that the timing during these events is essential to obtain a good performance score (Figure 3). The validation of the model shows similar performance.

Table 1. Performance index for the coupled Spatial Processes in Hydrology (SPHY)PCR-GLOBWB2 hydrological model on a daily time scale for 1989–1995 (calibration) and 1996–2000 (validation). The 95% quantiles represent $Q > Q_{95}^{th}$ ($4425 \text{ m}^3 \text{ s}^{-1}$) of the observed flow.

	Calibration		Validation	
	Full Time Series	95% Quantile	Full Time Series	95% Quantile
BIAS (%)	3.3	4.5	−0.8	7.3
NSE	0.78	0.31	0.64	0.3
RMSE (m^3s^{-1})	598	1475	650	1784
R^2	0.84	0.65	0.79	0.51

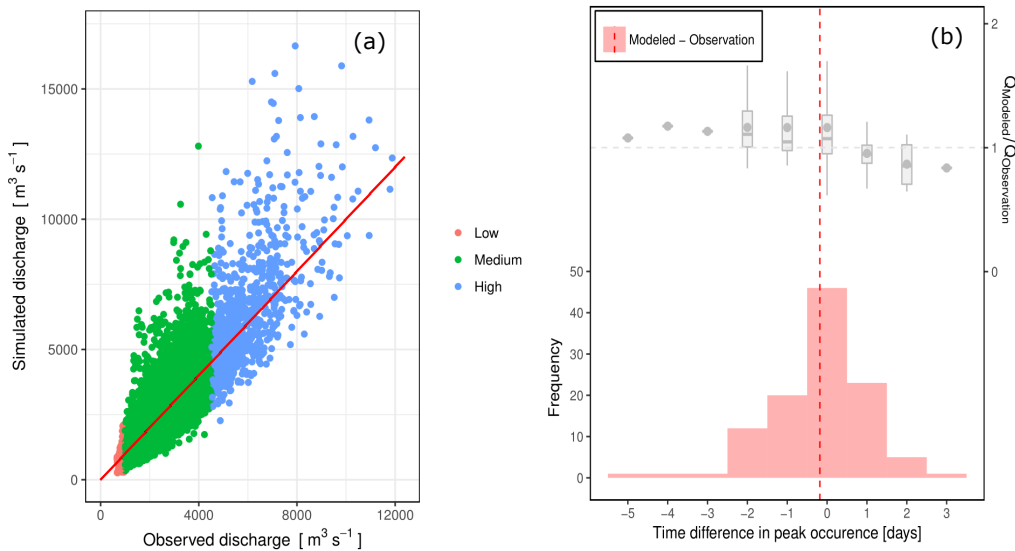


Figure 3. (a) Observed versus modelled daily discharge at Lobith for the period between 1951 and 2000. Colors indicate three ranges based on observed percentiles: Low (<5%, red), Medium (5%–95%, green) and High (>95%, blue). The solid red line represents the 1:1 slope. (b) Distribution of the difference between observed and modelled time of occurrence of discharge wave peak (red columns). The red dashed line represents the mean time error. The box plot represents the ratio of modeled and observed mean discharge for all wave peaks within a time difference interval. The grey line represents a mean ratio of 1. The grey point represents the mean of the ratio for each interval.

4.1.2. Flood Wave Timings

To assess the performance of the hydrological and routing model, the calibrated SPHY and routing models were forced with E-OBS daily precipitation and temperature data for the period 1951–2000. We evaluated the amplitude, timing and duration of extreme discharge events by using a simplified threshold approach to identify discharge waves [35]. A discharge (or flood wave) event is defined as a series of consecutive days (minimum of two days) with daily discharge exceeding the 95th quantile of the discharge. The length of each flood wave (in days) is calculated as the time difference between the onset (flow exceeds the threshold) and offset (flow falls below the threshold). Following this segregation method, we found 116 flood waves, on average just over two flood waves per year. The direct comparison of the timings for peak discharge (Figure 3b) shows that most of the simulated discharge waves reach the outlet at the same time as the observed discharge waves. Almost 80% of the flood waves reach the outlet within ± 1 day. Furthermore, the ratio between modelled and observed mean discharge is close to 1, suggesting that the wave volumes are estimated fairly well.

4.2. Snow Memory Effects

Figure 4a shows the effect of separating the snowfall events in low and high values on peak discharge. The years with above average snowfall tend to produce higher peak discharge than years with below

average snowfall. Longer return periods are dominated by the years with above average snowfall, and similarly below average snowfall corresponds to shorter return periods (Figure 4b). The ratio between the cumulative number of points below average and total show an exponential decay with increasing return time, confirming that higher discharges are dominated by above average snowfall years.

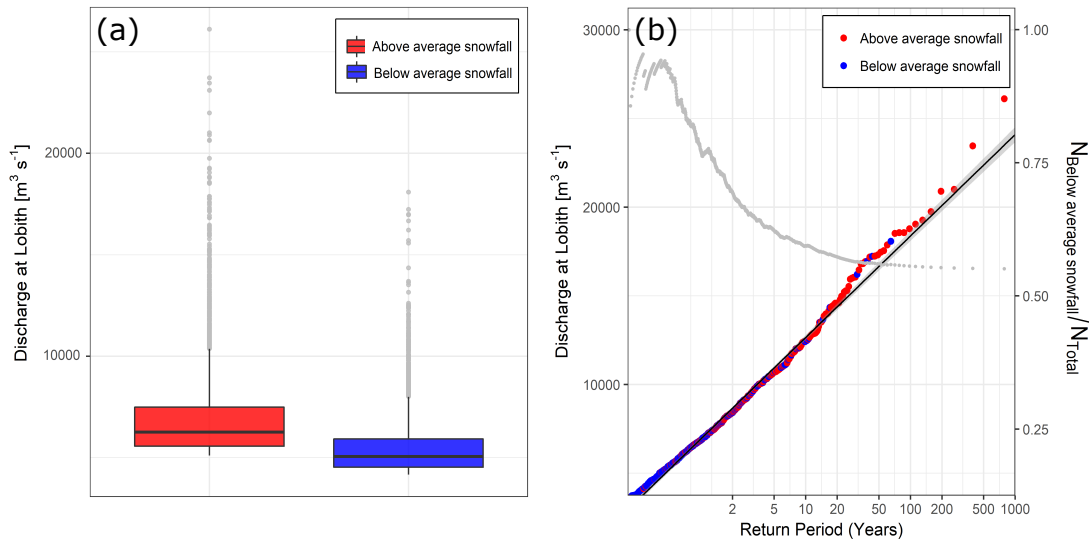


Figure 4. (a) Box plots for the discharge events exceeding the 95th quantiles for the year above and below average snowfall. (b) Generalized extreme value (GEV) plot of annual maximum discharge for years above and below average snowfall years. The grey point shows the fraction of below average snowfall samples. Its exponential decay shows a clear preference of below-normal snowfall events for the lower discharge return periods. The grey band around the line shows the confidence interval of the linear fit.

The seasonality of the snowfall and melting process play significant roles for the extent and seasonality of discharge extremes [69]. Figure 5 shows that years with above average snowfall have high discharge for January and February. The peak discharge regime is prolonged compared to years with below average snowfall. Snow accumulated in December in combination with fresh snow in January and February leads to this regime shift.

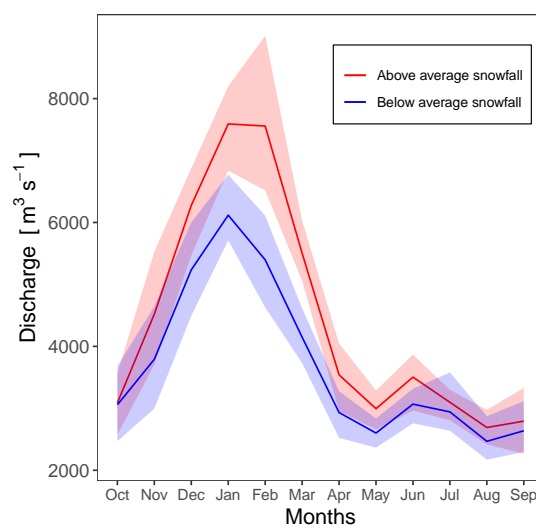


Figure 5. The seasonal cycle of discharge for the years above and below average snowfall. The solid lines are the mean of the 95th percentile of discharge for each ensemble member and the shaded area represents the spread of the ensemble (between 5th and 95th quantiles).

4.3. Soil Moisture Memory Effects

In summer, SM content is generally low. This gives a high infiltration capacity of the basin resulting in low to medium discharge response to extreme precipitation (Figure 6a). High SM is a default state in winter, which generates a stronger discharge response to precipitation (Figure 6b). The above analysis shows the effect of seasonal variation of SM on discharge, but significant variability in the SM–discharge–precipitation interaction prevails. To explore this interaction further, we applied a conditional sampling approach.

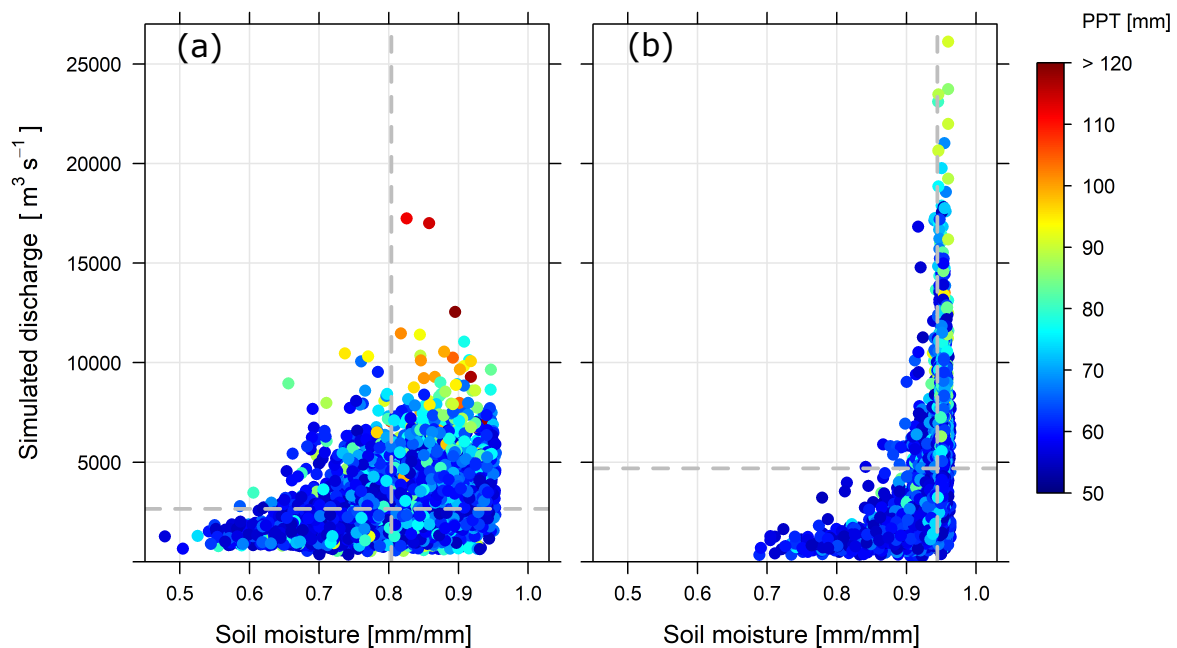


Figure 6. 10-day mean of soil moisture plotted against the corresponding discharge at the end of each 10 day interval, shown for 10-day precipitation events exceeding the 95% quantile for (a) summer (Mar–Sep) and (b) winter (Oct–Mar). The color scale represents the 10-day sum of precipitation (PPT) for the events shown. The dashed line represents the mean of the points for soil moisture and discharge.

Figure 7 shows that low precipitation on low initial SM results in the generation of low discharge values. The left two low precipitation (grey box plots within the red and blue partition) samples show the similar distribution implying that the discharges are solely driven by the SM conditions rather than the precipitation. The same applies for the right-hand side two high precipitation samples (grey box plots within the black and green partition). For both low and high precipitation values the effect of initial SM is evident: low SM values reduce the discharge volume strongly. Low precipitation on high SM results in higher discharge scenarios than high precipitation on low SM. SM controls the overland flow processes and is non-linearly related to the rainfall-runoff response [70,71]. High SM limits vertical infiltration in the soil, and precipitation will be routed towards saturation excess runoff triggering overland flow [72]. The results from this study are in line with the studies describing the antecedent SM controls on rainfall-runoff response [73–75].

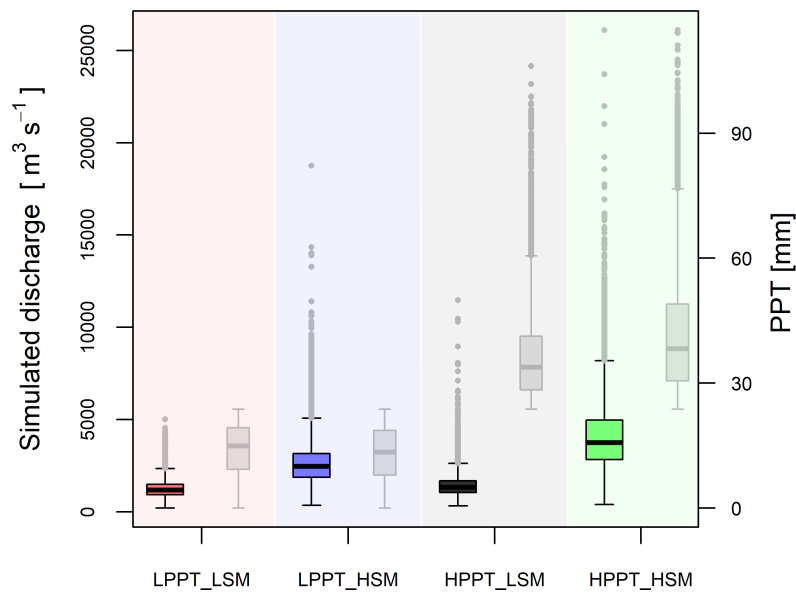


Figure 7. Simulated discharges for four different sampling scenarios: LPPT_LSM indicates below median 10-day precipitation in combination with climatological low initial soil moisture (<10% quantile), HPPT_HSM high precipitation/high soil moisture (>90% quantile), and HPPT_LSM and LPPT_HSM show corresponding combinations. The colored boxes show the distribution of discharge in each bin, the grey boxes the distribution of 10-day precipitation sums (right axis scale).

4.4. Meteorological Autocorrelation

4.4.1. Importance of Autocorrelation

The role of autocorrelation between meteorological events is shown in Figure 8 and Table 2, demonstrating the significance of meteorological memory for extreme hydrological events. Removing the memory in the meteorological system (shuffled time series using a one-day block; red line) reduces the slope of generalized extreme value (GEV) annual maximum discharge distribution down to 45% of the original non-shuffled simulation (black line), e.g., the associated peak discharge becomes 45% lower.

Removing all correlation at length scales exceeding a single day leads to a GEV slope that is more than 50% lower than the original (Table 2). This shows that high discharge peaks originate from multi-day precipitation events, generated by synoptic systems that generate rainfall for a subsequent period of time. Indeed, preserving the meteorological memory for five days retains almost 80% of the original GEV slope. This is a time scale that can be associated with large low pressure systems that are slowly moving over the basin. Virtually all peak discharge events are well reproduced when autocorrelation at the monthly timescale is retained. Shuffling the data with half-yearly blocks increases the GEV slope slightly, but primarily by generating lower discharge at low return periods (see Figure 8). Differences in the model runs are mainly due to the other memory processes in the hydrological system such as snowfall, SM, and snowmelt.

The monotonic decrease in maximum discharge with incremental reductions in the block length shows a relatively large step (from 0.78 to 0.46) timescales of one and five days (Table 2). This implies that most of the memory in the meteorological system in the Rhine basin is present at time scales around five days. This includes the possibility of high discharge events affected by sequences of storms. Memory characteristics at longer time scales can also include effects of accumulating snow, SM and groundwater processes. Particularly the difference between retaining 10-day or 30-day memory is related to snow processes. At this timescale, snow in the higher Alpine areas of the Rhine can be stored. At the half-yearly time scale the seasonal cycle of snow accumulation and ablation, and the dynamics of SM storage, become prominent.

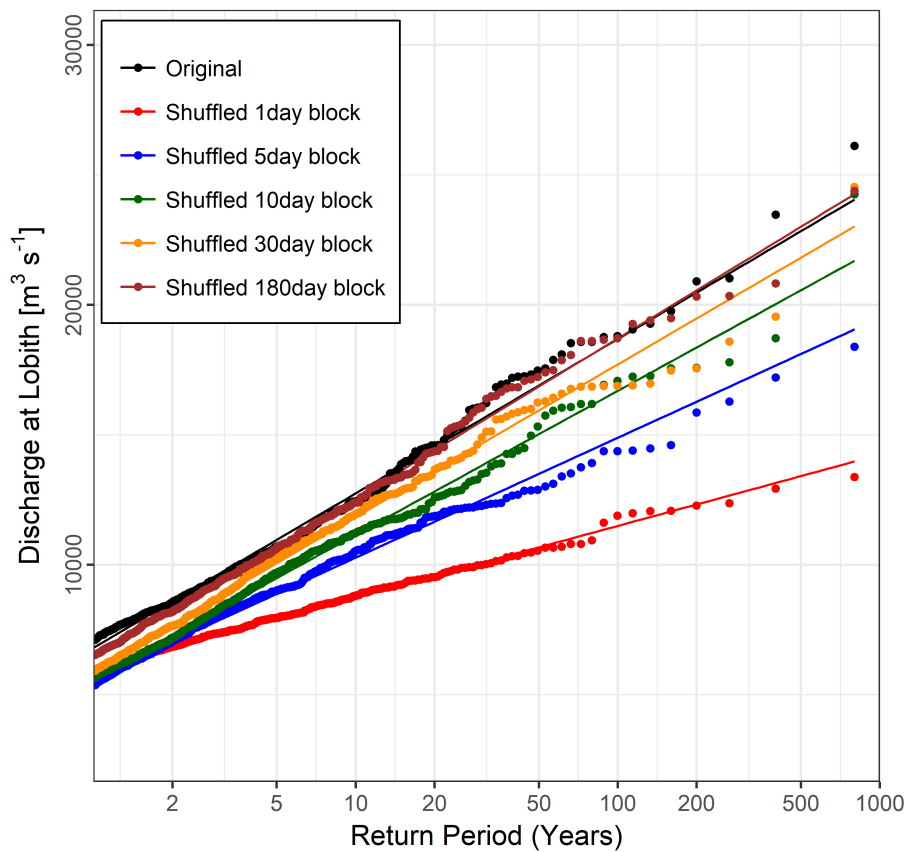


Figure 8. GEV fit of annual maxima discharges of the different meteorological shuffling experiments. The points (colored) represent the distribution and the solid (colored) line represent the linear fit on a logarithmic scale.

Table 2. Slope of the GEV shown in Figure 8, and lower and upper bound of the linear fit. Results are normalized relative to the original unshuffled simulation.

Shuffling	Slope	Lower Bound	Upper Bound
Original	1	0.978	1.022
Shuffled 1 day block	0.462	0.457	0.467
Shuffled 5 days block	0.777	0.761	0.793
Shuffled 10 days block	0.933	0.916	0.949
Shuffled 30 days block	0.99	0.972	1.008
Shuffled 180 days block	1.035	0.995	1.049

4.4.2. Case Studies

For a number of hydrological extreme events we analyzed the synoptic meteorological patterns leading up to these events, and how the events develop in time. Following earlier studies exploring the relation between peak discharge from the Rhine and the precipitation time scale [33,34,76,77], we analyzed the meteorological situation for the 10-day period preceding an extreme discharge event. Anomalous circulation characteristics and associated land surface fields were evaluated for extreme discharge events, both for the original and for the shuffled (one-day block) simulations. The comparison of these anecdotal situations was carried out for the most extreme events in these two simulations.

Floods occurring during the winter half of the year in the western part of Europe are primarily due to zonal westerly circulation systems [78]. Synoptically the most extreme event in the standard simulation is characterized by a strong low-pressure system moving from Iceland to the Scandinavian region [33]. The persistent low pressure over the Iceland region results in development of strong

westerly winds. These are characterized by humid Atlantic moisture conditions and transport moisture towards the Alps (Figure 9a). The climatological flow of the period in which this event took place has a more south westerly direction resulting in less rainfall than during the event (Figure 9b). The patches of high precipitation in the upper Rhine and Alpine regions are aligned with the N-S orientation of the Black forest and Vosges mountain range (Figure 9c). The moisture laden westerlies result in topographically induced rainfall and snowfall in the mountainous region of the Black forest and Alps (Figure 9d,e).

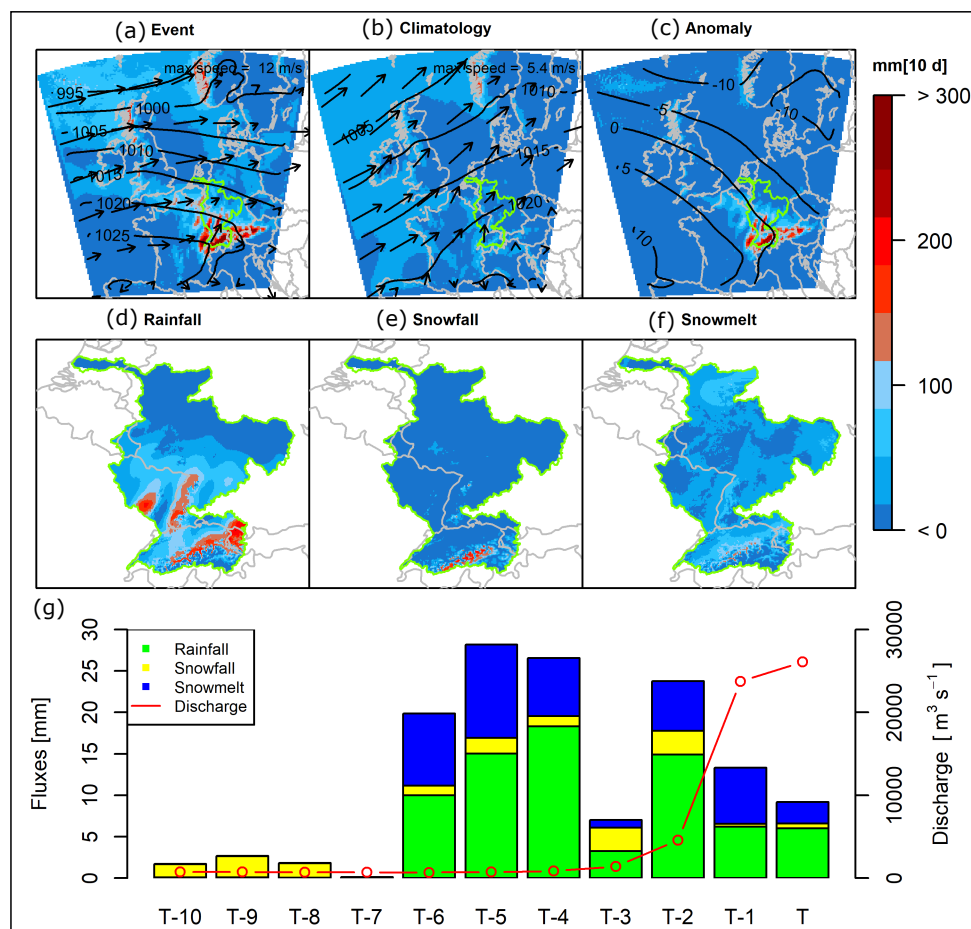


Figure 9. Meteorological circulation patterns leading up to the most extreme discharge event in the control simulation (date: 1953-12-27; member 10). Fields shown are composed of 10-day mean sea level pressure (SLP) and near surface wind and 10-day accumulated precipitation, rainfall, snowfall and snowmelt. Panel (a) shows the accumulated 10-day precipitation during the event together with the 10-day mean wind (arrows) and SLP (contours). Panel (b) shows the climatology of the event for the same 10-day episode in the ensemble. Panel (c) shows the anomaly of the event. Panels (d–f) show the rainfall, snowfall and snowmelt anomalies respectively. Panel (g) shows the sums of basin mean daily averaged fluxes of the hydrological budget terms during the event (colored bars) together with discharge (red line).

In the shuffled simulations the circulation anomalies for the most extreme event are much less pronounced than in the control simulation (Figure 10a). The south westerly winds are aligned parallel to the mountain ranges and result in less precipitation than the winds in the control simulation that are aligned nearly perpendicular to the mountains. The rainfall anomalies are positive mainly in the middle Rhine, Cochem and Main catchments (Figure 10d). Conversely, there are no significant differences in snowfall and snow melt anomalies in the region.

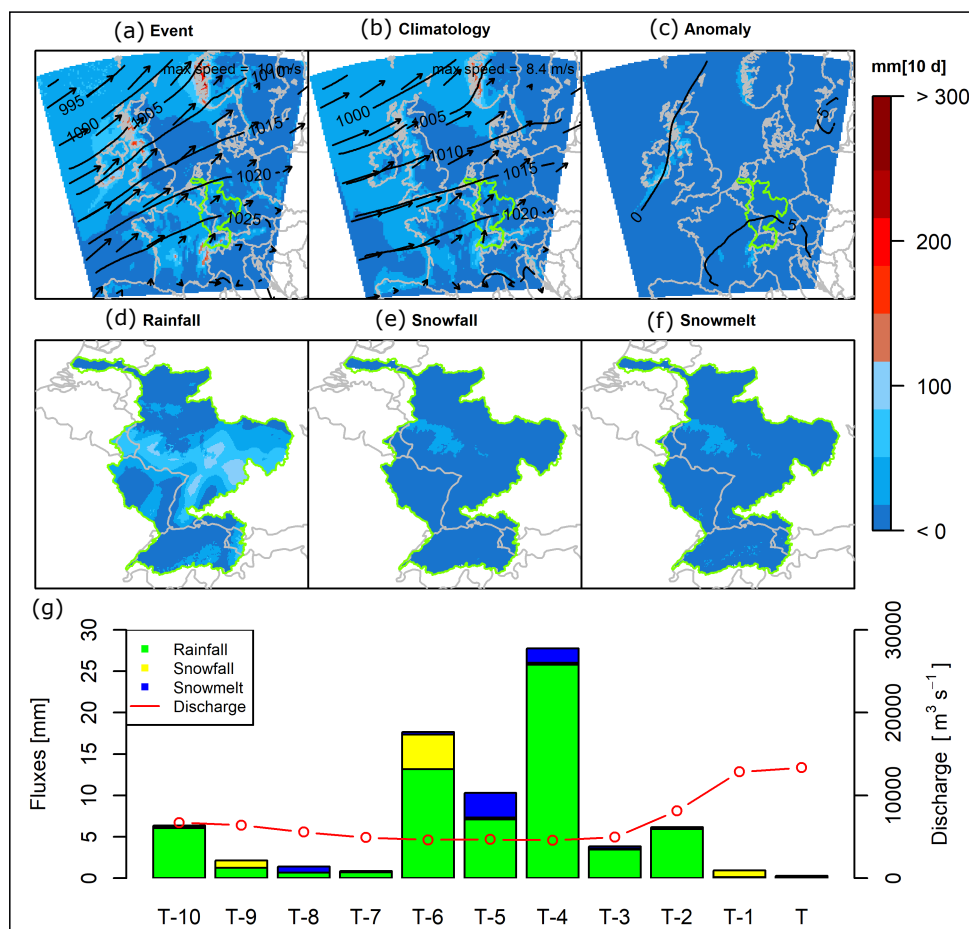


Figure 10. As for Figure 9, for the most extreme event in the one-day block shuffled simulation (date: 1982-01-15; member 12).

The temperature evolution 10 days prior to the event reveals that most of the region is cold (below 0 °C) for multiple days early in that period (Figure S1a), thus resulting in precipitation falling as snow (Figure 9g). The precipitation event, mainly characterized by the sequence of moderate rainfall episodes, continued for about six days prior to the extreme discharge event. Accumulated snowfall at T-10 to T-8 served as a source of snow melt later in the period, when temperatures reached values above 0 °C. Snowmelt thus occurred jointly with snow/rain and contributed to the peak discharge (Figure S1b). In some areas (mainly higher alpine regions and the Neckar region) low temperatures prevailed during the entire 10 day period thus triggering rain on snow processes. A saturated antecedent SM state, which is normal in this time of the year (Figure S3) aggravated the magnitude of the discharge generating processes [69,79,80]. Therefore, the coincidence of persistent meteorological patterns resulting in multiple episodes of rainfall events, warmer temperature activating snow melt, high antecedent SM in combination with rain on snow processes, and preceded by several days of snowfall together resulted in an extreme discharge event.

Contrary to the extreme discharge generation mechanism from the control simulation, shuffled simulations show a different magnitude and different types of discharge generation processes (Figure 10). The striking difference in magnitude of the discharge peak is notable (Figure 10g). The complete removal of memory from precipitation resulted in the reduction of the discharge peak by nearly 50%. The precipitation is mostly in the form of rain except for six days prior to the peak discharge event, consistent with the evolution of the region’s temperature (Figure S2). The lower and middle part of the Rhine experience cold temperatures and this results in the accumulation of snowfall. The temperature throughout the basin is found to be above zero except one day before the discharge

event. The event is solely dominated by rainfall-runoff mechanism. The rainfall event stretching for multiple days in combination with the saturated antecedent SM (Figure S4) generates the peak discharge. The snow memory effect hardly plays a role in this event.

5. Discussion and Conclusions

Though this study overcomes the limitations posed on the past studies for instance limited observation records, reanalysis products or model simulations, and/or focusing on a limited dynamic range of the lagged signals contributing to the CEs, it still has a number of potential caveats. First, the analysis is based on the cascade of meteorological, hydrological and routing models, which all are imperfect and biased. Downscaling of GCM simulations may impart the extreme meteorological signal [81–83]. The choice of routing scheme has a considerable influence on the timing of simulated river discharge and its peak values [84–86]. Furthermore, the limitations in the hydrological model structure and hydraulic model to correctly simulate the timing and magnitude of flood waves add to the uncertainty from downscaling of climate data [87–90].

The meteorological shuffling represents a combination of, and interaction between, memory from the meteorological and hydrological systems. To exclusively isolate the contribution of hydrological memory from the meteorological memory a random SM or snow storage state could be considered at each time step of the model run. This ensures that any system memory in the hydrological system is removed, and remaining memory is resulting from the meteorological autocorrelation. The riverine memory, for instance off-channel, canals, lakes and reservoir storages of the hydrological systems, are not modeled in this study. Though the ground water interacts and modulates with the SM and base flow, the explicit contribution to the peak generation is not assessed. The ground water memory [1,10,11,91], a contributing memory component for the generation of extreme flood in Rhine [92], is not directly attributed here. Further, the SM calculations are only limited to the top rootzone layer and it lacks the effects of progressively deeper SM memory processes.

The most extreme discharge in the control simulations (representative for a return period of once in 800 years) at Lobith is around $26,000 \text{ m}^3\text{s}^{-1}$ which is around 50% higher than the current design discharge of $18,000 \text{ m}^3\text{s}^{-1}$ (for a return period of once in 1250 years) [49]. This high estimate can be partly attributed to biases in EOBS, calibration of the hydrological and hydraulic model and the atmospheric models used in the study. However, the high estimate could also be the result of an unprecedented extreme event that has not been realized in the limited observational records and cannot be estimated by extrapolation of the observational record. The use of a large ensemble overcomes this limitation posed by the short-term observations and therefore the possibility of occurrence of such an extreme event cannot be neglected. Additionally, the systematic biases are not expected to have a large impact on the correlation structures of the processes and events studied here.

The findings confirm that the years with annual snowfall above average tend to generate anomalous high discharge. The snow accumulated in the basin serves as an additional source of meltwater for the discharge resulting in a significant shift of the discharge peak. A strong asymmetric rainfall-runoff response is triggered by the sensitivity to the initial SM state. Additionally, our results show that meteorological autocorrelation has a strong impact on the magnitude of peak discharge. The higher discharge peaks tend to level off (flatter slopes) in the hypothetical and shuffled weather scenarios where all the correlations in the meteorology are removed. The shuffling randomizes the sequence of the weather events, and thus deletes the memory of the meteorological system. A monotonic increment in extreme discharges with longer memory time scales is found. The results highlight that removing any meteorological autocorrelation occurring at time scales longer than five days reduces peak discharge by 80% relative to the control simulations. Autocorrelation at time scales longer than 30 days plays a minor role. Most memory in the meteorological system in the Rhine basin is found at time scales around five days. Furthermore, we show how hydrological memory from snow accumulation and SM complements the generation of extreme discharges. These findings are relevant when exploring the effect of extreme discharge events that are caused by a compound occurrence of

drivers. The time scales identified do diagnose the time scale at which compounding drivers need to be considered in order to contribute to a meaningful analysis of compound events.

Supplementary Materials: The following are available online at <http://www.mdpi.com/2073-4433/10/4/171/s1>.

Author Contributions: Conceptualization, S.K. and B.v.d.H.; Data curation, S.K.; Formal analysis, S.K.; Funding acquisition, B.v.d.H.; Investigation, S.K.; Methodology, S.K., A.F.L., W.W.I. and H.d.V.; Project administration, S.K.; Resources, S.K. and N.W.; Software, S.K. and N.W.; Supervision, A.F.L., W.W.I. and B.v.d.H.; Validation, S.K.; Visualization, S.K.; Writing—original draft, S.K.; Writing—review & editing, S.K., A.F.L., W.W.I., H.d.V. and N.W.

Funding: This research was funded by the European Union’s Horizon 2020 research and innovation programme under the Marie Skłodowska-Curie grant agreement No 676027. The project has also received funding from the European Research Council (ERC) under the European Union’s Horizon 2020 research and innovation program (grant agreement number 676819) and the Netherlands Organization for Scientific Research under the Innovational Research Incentives Scheme VIDI (grant agreement 016.181.308).

Acknowledgments: The authors would like to thank the IMPREX project, in particular Erik van Meijgaard, for providing the downscaled RACMO simulations. The authors would like to acknowledge Nina Ridder for her contribution to discussions during this study.

Data availability: The code of the SPHY model is publicly available at <https://github.com/FutureWater/SPHY>. The PCR-GLOBWB 2.0 model is publicly available at https://github.com/UU-Hydro/PCR-GLOBWB_model. The datasets that are produced in this study are available upon request from the corresponding author.

Conflicts of Interest: The authors declare no conflict of interest.

References

1. Wu, W.; Dickinson, R.E. Time scales of layered soil moisture memory in the context of land-atmosphere interaction. *J. Clim.* **2004**, *17*, 2752–2764. [[CrossRef](#)]
2. Vinnikov, K.Y.; Robock, A.; Speranskaya, N.A.; Schlosser, C.A. Scales of temporal and spatial variability of midlatitude soil moisture. *J. Geophys. Res.* **1996**, *101*, 7163–7174. [[CrossRef](#)]
3. Entin, J.K.; Robock, A.; Vinnikov, K.Y.; Hollinger, S.E.; Liu, S.; Namkhai, A. Meteorologic i Land Surface. *J. Geophys. Res.* **2000**, *105*, 11865–11877. [[CrossRef](#)]
4. Lorenz, E.N. The predictability of a flow which possesses many scales of motion. *Tellus* **1969**, *21*, 289–307. [[CrossRef](#)]
5. Pelletier, J.D.; Turcotte, D.L. Long-range persistence in climatological and hydrological time series: Analysis, modeling and application to drought hazard assessment. *J. Hydrol.* **1997**, *203*, 198–208. [[CrossRef](#)]
6. Wanders, N.; Thober, S.; Kumar, R.; Pan, M.; Sheffield, J.; Samaniego, L.; Wood, E.F. Development and evaluation of a Pan-European multi-model seasonal hydrological forecasting system. *J. Hydrometeorol.* **2019**, *20*, 99–115. [[CrossRef](#)]
7. Koutsoyiannis, D. Hydrologic Persistence and The Hurst Phenomenon. *Water Encycl.* **2005**. [[CrossRef](#)]
8. Delworth, T.L.; Manabe, S. The Influence of Potential Evaporation on the Variabilities of Simulated Soil Wetness and Climate. *J. Clim.* **1988**, *1*, 523–547. [[CrossRef](#)]
9. Scott, R.; Entekhabi, D.; Koster, R.; Suarez, M. Timescales of land surface evapotranspiration response. *J. Clim.* **1997**, *10*, 559–566. [[CrossRef](#)]
10. Amenu, G.G.; Kumar, P.; Liang, X.-Z. Interannual Variability of Deep-Layer Hydrologic Memory and Mechanisms of Its Influence on Surface Energy Fluxes. *J. Clim.* **2005**, *18*, 5024–5045. [[CrossRef](#)]
11. Güntner, A.; Stuck, J.; Werth, S.; Döll, P.; Verzano, K.; Merz, B. A global analysis of temporal and spatial variations in continental water storage. *Water Resour. Res.* **2007**, *43*, 1–19. [[CrossRef](#)]
12. Seneviratne, S.I.; Koster, R.D. A Revised Framework for Analyzing Soil Moisture Memory in Climate Data: Derivation and Interpretation. *J. Hydrometeorol.* **2012**, *13*, 404–412. [[CrossRef](#)]
13. Bojariu, R.; Gimeno, L. The role of snow cover fluctuations in multiannual NAO persistence. *Geophys. Res. Lett.* **2003**, *30*, 1–4. [[CrossRef](#)]
14. Cohen, J.; Fletcher, C. Improved skill of northern hemisphere winter surface temperature predictions based on land-atmosphere fall anomalies. *J. Clim.* **2007**, *20*, 4118–4132. [[CrossRef](#)]
15. Xu, L.; Dirmeyer, P. Snow-atmosphere coupling strength in a global atmospheric model. *Geophys. Res. Lett.* **2011**, *38*. [[CrossRef](#)]
16. Hurst, H.E. Long-term storage capacity of reservoirs. *Trans. Am. Soc. Civ. Eng.* **1951**, *116*, 770–808.

17. Montanari, A.; Rosso, R.; Taqqu, M.S. Fractionally differenced ARIMA models applied to hydrologic time series: Identification, estimation, and simulation. *Water Resour. Res.* **1997**, *33*, 1035–1044. [[CrossRef](#)]
18. Koutsoyiannis, D. The Hurst phenomenon and fractional Gaussian noise made easy The Hurst phenomenon and fractional Gaussian noise made easy. *Hydrol. Sci. J.* **2002**, *47*, 573–595. [[CrossRef](#)]
19. Blender, R.; Fraedrich, K. Long-term memory of the hydrological cycle and river runoffs in China in a high-resolution climate model. *Int. J. Climatol.* **2006**, *26*, 1547–1565. [[CrossRef](#)]
20. Mudelsee, M.; Borngen, M.; Tetzlaff, G.; Grunewald, U. No Upward Trends In The Occurrence Of Extreme Floods In Central Europe. *Nature* **2003**, *425*, 166–169. [[CrossRef](#)]
21. Bunde, A.; Eichner, J.F.; Kantelhardt, J.W.; Havlin, S. Long-term memory: A natural mechanism for the clustering of extreme events and anomalous residual times in climate records. *Phys. Rev. Lett.* **2005**, *94*, 1–4. [[CrossRef](#)] [[PubMed](#)]
22. Koster, R.D.; Suarez, M.J. Soil Moisture Memory in Climate Models. *J. Hydrometeorol.* **2001**, *2*, 558–570. [[CrossRef](#)]
23. Orth, R.; Seneviratne, S.I. Analysis of soil moisture memory from observations in Europe. *J. Geophys. Res. Atmos.* **2012**, *117*, 1–19. [[CrossRef](#)]
24. Dirmeyer, P.A.; Schlosser, C.A.; Brubaker, K.L. Precipitation, Recycling, and Land Memory: An Integrated Analysis. *J. Hydrometeorol.* **2009**, *10*, 278–288. [[CrossRef](#)]
25. Bierkens, M.F.P.; van den Hurk, B.J.J.M. Groundwater convergence as a possible mechanism for multi-year persistence in rainfall. *Geophys. Res. Lett.* **2007**, *34*, 1–5. [[CrossRef](#)]
26. Van Lanen, H.A.J.; Wanders, N.; Tallaksen, L.M.; Van Loon, A.F. Hydrological drought across the world: Impact of climate and physical catchment structure. *Hydrol. Earth Syst. Sci.* **2013**, *17*, 1715–1732. [[CrossRef](#)]
27. Shinoda, M. Climate memory of snow mass as soil moisture over central Eurasia. *J. Geophys. Res. Atmos.* **2001**, *106*, 33393–33403. [[CrossRef](#)]
28. Cohen, J.; Rind, D. The Effect of Snow Cover on the Climate. *J. Clim.* **1991**, *4*, 689–706. [[CrossRef](#)]
29. Zscheischler, J.; Westra, S.; Van Den Hurk, B.J.J.M.; Seneviratne, S.I.; Ward, P.J.; Pitman, A.; Aghakouchak, A.; Bresch, D.N.; Leonard, M.; Wahl, T.; et al. Future climate risk from compound events. *Nat. Clim. Chang.* **2018**, *8*, 469–477. [[CrossRef](#)]
30. Nicholson, S.E. Land Surface Processes and Land Use Change Land. *Rev. Geophys.* **2000**, *38*, 117–139. [[CrossRef](#)]
31. Bonan, G.B.; Stillwell-soller, L.M. Soil water and the persistence of floods and droughts in the Mississippi River Basin. *Water Resour. Res.* **1998**, *34*, 2693–2701. [[CrossRef](#)]
32. Liu, D.; Wang, G.; Mei, R.; Yu, Z.; Yu, M. Impact of initial soil moisture anomalies on climate mean and extremes over Asia. *J. Geophys. Res.* **2014**, *119*, 529–545. [[CrossRef](#)]
33. van den Hurk, B.; van Meijgaard, E.; de Valk, P.; van Heeringen, K.-J.; Gooijer, J. Analysis of a compounding surge and precipitation event in the Netherlands. *Environ. Res. Lett.* **2015**, *10*, 035001. [[CrossRef](#)]
34. Kew, S.F.; Selten, F.M.; Lenderink, G.; Hazeleger, W. The simultaneous occurrence of surge and discharge extremes for the Rhine delta. *Nat. Hazards Earth Syst. Sci.* **2013**, *13*, 2017–2029. [[CrossRef](#)]
35. Khanal, S.; Ridder, N.; de Vries, H.; Terink, W.; van den Hurk, B. Storm surge and extreme river discharge: A compound event analysis using ensemble impact modelling. *Hydrol. Earth Syst. Sci. Discuss.* **2018**. [[CrossRef](#)]
36. Leonard, M.; Westra, S.; Phatak, A.; Lambert, M.; van den Hurk, B.; McInnes, K.; Risbey, J.; Schuster, S.; Jakob, D.; Stafford-Smith, M. A compound event framework for understanding extreme impacts. *Wiley Interdiscip. Rev. Clim. Chang.* **2014**, *5*, 113–128. [[CrossRef](#)]
37. Wahl, T.; Haigh, I.D.; Nicholls, R.J.; Arns, A.; Dangendorf, S.; Hinkel, J.; Slangen, A.B.A. Understanding extreme sea levels for broad-scale coastal impact and adaptation analysis. *Nat. Commun.* **2017**, *8*, 16075. [[CrossRef](#)] [[PubMed](#)]
38. Hazeleger, W.; van den Hurk, B.J.J.M.; Min, E.; van Oldenborgh, G.J.; Petersen, A.C.; Stainforth, D.A.; Vasileiadou, E.; Smith, L.A. Tales of future weather. *Nat. Clim. Chang.* **2015**, *5*, 107–113. [[CrossRef](#)]
39. Seneviratne, S.; Nicholls, N.; Easterling, D.; Goodess, C.; Kanae, S.; Kossin, J.; Luo, Y.; Marengo, J.; McInnes, K.; Rahimi, M.; et al. Changes in climate extremes and their impacts on the natural physical environment. *Manag. Risk Extrem. Events Disasters to Adv. Clim. Chang. Adapt.* **2012**, 109–230.
40. Ridder, N.; de Vries, H.; Drijfhout, S. The Role of Atmospheric Rivers in compound events consisting of heavy precipitation and high storm surges along the Dutch coast. *Nat. Hazards Earth Syst. Sci. Discuss.* **2018**, *18*, 3311–3326. [[CrossRef](#)]

41. Klerk, W.J.; Winsemius, H.C.; van Verseveld, W.J.; Bakker, A.M.R.; Diermanse, F.L.M. The co-occurrence of storm surges and extreme discharges within the Rhine–Meuse Delta. *Environ. Res. Lett.* **2015**, *10*, 035005. [[CrossRef](#)]
42. Pinter, N.; Van der Ploeg, R.R.; Schweigert, P.; Hofer, G. Flood magnification on the River Rhine. *Hydrol. Process.* **2006**, *20*, 147–164. [[CrossRef](#)]
43. Te Linde, A.H.; Aerts, J.C.J.H.; Bakker, A.M.R.; Kwadijk, J.C.J. Simulating low-probability peak discharges for the Rhine basin using resampled climate modeling data. *Water Resour. Res.* **2010**, *46*, 1–19. [[CrossRef](#)]
44. Junghans, N.; Cullmann, J.; Huss, M. Evaluating the effect of snow and ice melt in an Alpine headwater catchment and further downstream in the River Rhine. *Hydrol. Sci. J.* **2011**, *56*, 981–993. [[CrossRef](#)]
45. Stahl, K.; Weiler, M.; Kohn, I.; Freudiger, D.; Seibert, J.; Vis, M.; Gerlinger, K. The snow and glacier melt components of streamflow of the river Rhine and its tributaries considering the influence of climate change. Available online: <https://www.chr-khr.org/en/publication/snow-and-glacier-melt-components-streamflow-river-rhine-and-its-tributaries-considerin-0> (accessed on 31 March 2019).
46. Engel, H. The flood events of 1993/1994 and 1995 in the Rhine River basin. In *Destructive Water: Water-Caused Natural Disasters, Their Abatement and Control*; IAHS Publication No 239; Leavesly, G.H., Lins, H.F., Nobilis, F., Parker, R.S., Schneider, V.R., Van de Ven, F.H.M., Eds.; IAHS Press: Wallingford, UK, 1997; pp. 21–32.
47. Disse, M.; Engel, H. Flood events in the Rhine basin: Genesis, influences and mitigation. *Nat. Hazards* **2001**, *23*, 271–290. [[CrossRef](#)]
48. Kew, S.F.; Selten, F.M.; Lenderink, G.; Hazeleger, W. Robust assessment of future changes in extreme precipitation over the Rhine basin using a GCM. *Hydrol. Earth Syst. Sci.* **2011**, *15*, 1157–1166. [[CrossRef](#)]
49. Hegnauer, M.; Kwadijk, J.; Klijn, F. *The Plausibility of Extreme High Discharges in the River Rhine*; Deltares: Delft, The Netherlands, 2015.
50. Minville, M.; Velázquez, J.A.; Gauvin St-Denis, B.; Muerth, M.J.; Schmid, J.; Chaumont, D.; Ludwig, R.; Caya, D.; Turcotte, R.; Ricard, S. On the need for bias correction in regional climate scenarios to assess climate change impacts on river runoff. *Hydrol. Earth Syst. Sci.* **2013**, *17*, 1189–1204.
51. Brienen, S.; Rust, H.W.; Sauter, T.; Themeßl, M.; Venema, V.K.C.; Chun, K.P.; Maraun, D.; Wetterhall, F.; Ireson, A.M.; Chandler, R.E.; et al. Precipitation Downscaling Under Climate Change: Recent Developments To Bridge the Gap Between Dynamical Models and the End User. *Rev. Geophys.* **2010**, *48*, 1–34.
52. Kleinn, J.; Frei, C.; Gurtz, J.; Lüthi, D.; Vidale, P.L.; Schär, C. Hydrologic simulations in the Rhine basin driven by a regional climate model. *J. Geophys. Res. D Atmos.* **2005**, *110*, 1–18. [[CrossRef](#)]
53. Viviroli, D.; Messerli, B. Assessing the Hydrological Significance of the World’s Mountains. *Mt. Res. Dev.* **2003**, *23*, 369–375. [[CrossRef](#)]
54. Photiadou, C.S.; Weerts, A.H.; Van Den Hurk, B.J.J.M. Evaluation of two precipitation data sets for the Rhine River using streamflow simulations. *Hydrol. Earth Syst. Sci.* **2011**, *15*, 3355–3366. [[CrossRef](#)]
55. Kwadijk, J.; Van Deursen, W. *Internationale Kommission für die Hydrologie des Rheingebietes Commission Internationale de l’Hydrologie du Bassin du Rhin Development and Testing of a GIS Based Water Balance Model for the Rhine Drainage Basin*; Utrecht University: Utrecht, The Netherlands, 1999.
56. Hegnauer, M.; Beersma, J.J.; van den Boogaard, H.F.P.; Buishand, T.A.; Passchier, R.H. *Generator of Rainfall and Discharge Extremes (GRADE) for the Rhine and Meuse Basins*; Final Report of GRADE 2.0; Deltares: Delft, The Netherlands, 2014.
57. Ward, P.J.; Jongman, B.; Aerts, J.C.J.H.; Bates, P.D.; Botzen, W.J.W.; Diaz Loaiza, A.; Hallegatte, S.; Kind, J.M.; Kwadijk, J.; Scussolini, P.; et al. A global framework for future costs and benefits of river-flood protection in urban areas. *Nat. Clim. Chang.* **2017**, *7*, 642. [[CrossRef](#)]
58. Hazeleger, W.; Wang, X.; Severijns, C.; Ştefănescu, S.; Bintanja, R.; Sterl, A.; Wyser, K.; Semmler, T.; Yang, S.; van den Hurk, B.; et al. EC-Earth V2.2: Description and validation of a new seamless earth system prediction model. *Clim. Dyn.* **2012**, *39*, 2611–2629. [[CrossRef](#)]
59. van Meijgaard, E.; Uft, L.H. Van; Bosveld, F.C.; Lenderink, G.; Siebesma, A.P. *The KNMI Regional Atmospheric Climate Model RACMO Version 2.1*; Technical Report, TR-302; The Royal Netherlands Meteorological Institute: De Bilt, Netherlands, 2008; p. 43.
60. Haylock, M.R.; Hofstra, N.; Klein Tank, A.M.G.; Klok, E.J.; Jones, P.D.; New, M. A European daily high-resolution gridded data set of surface temperature and precipitation for 1950–2006. *J. Geophys. Res. Atmos.* **2008**, *113*. [[CrossRef](#)]

61. Terink, W.; Lutz, A.F.; Simons, G.W.H.; Immerzeel, W.W.; Droogers, P. SPHY: Spatial Processes in Hydrology. *Geosci. Model Dev. Discuss.* **2015**, *8*, 1687–1748. [[CrossRef](#)]
62. Hock, R. Temperature index melt modelling in mountain areas. *J. Hydrol.* **2003**, *282*, 104–115. [[CrossRef](#)]
63. Hargreaves, G.H.; Samani, Z.A. Reference Crop Evapotranspiration from Temperature. *Appl. Eng. Agric.* **2013**, *1*, 96–99. [[CrossRef](#)]
64. Sutanudjaja, E.H.; Van Beek, R.; Wanders, N.; Wada, Y.; Bosmans, J.H.C.; Drost, N.; Van Der Ent, R.J.; De Graaf, I.E.M.; Hoch, J.M.; De Jong, K.; et al. PCR-GLOBWB 2: A 5 arcmin global hydrological and water resources model. *Geosci. Model Dev.* **2018**, *11*, 2429–2453. [[CrossRef](#)]
65. GRDC. Available online: http://www.bafg.de/GRDC/EN/01_GRDC/grdc_node.html (accessed on 1 November 2016).
66. Rajagopalan, B.; Lall, U. A k-nearest-neighbor Simulator for Daily Precipitation and Other Variables. *Water Resour. Res.* **1999**, *35*, 3089–3101. [[CrossRef](#)]
67. Beersma, J. *Extreme Hydro-Meteorological Events and Their Probabilities*; Wageningen University: Wageningen, The Netherlands, 2007; ISBN 9085046157.
68. Nash, J.E.; Sutcliffe, J.V. River Flow Forecasting Through Conceptual Models Part I—a Discussion of Principles. *J. Hydrol.* **1970**, *10*, 282–290. [[CrossRef](#)]
69. Sivapalan, M.; Blöschl, G.; Merz, R.; Gutknecht, D. Linking flood frequency to long-term water balance: Incorporating effects of seasonality. *Water Resour. Res.* **2005**, *41*, 1–17. [[CrossRef](#)]
70. Zehe, E.; Sivapalan, M. Threshold behaviour in hydrological systems as (human) geo-ecosystems: Manifestations, controls, implications. *Hydrol. Earth Syst. Sci.* **2009**, *13*, 1273–1297. [[CrossRef](#)]
71. Mcgrath, G.S.; Hinz, C.; Sivapalan, M.; Mcgrath, G.S.; Hinz, C.; Temporal, M.S. Temporal dynamics of hydrological threshold events To cite this version: Temporal dynamics of hydrological threshold events. *Hydrol. Earth Syst. Sci. Discuss.* **2007**, *11*, 923–938.
72. Dunne, T. Field Studies of Hillslope Flow Processes. *Hillslope Hydrol.* **1978**, 227–293. [[CrossRef](#)]
73. Blöschl, G.; Zehe, E. On hydrological predictability. *Hydrol. Process.* **2005**, *19*, 3923–3929. [[CrossRef](#)]
74. Zehe, E.; Graeff, T.; Morgner, M.; Bauer, A.; Bronstert, A. Plot and field scale soil moisture dynamics and subsurface wetness control on runoff generation in a headwater in the Ore Mountains. *Hydrol. Earth Syst. Sci.* **2010**, *14*, 873–889. [[CrossRef](#)]
75. Beven, K. Robert E. Horton’s perceptual model of infiltration processes. *Hydrol. Process.* **2004**, *18*, 3447–3460. [[CrossRef](#)]
76. Beersma, J.J.; Kwadijk, J.C.J.; Lammersen, R. *Effects of Climate Change on the Rhine Discharges*; Deltares: Delft, The Netherlands, 2008.
77. van den Brink, H.W.; Können, G.P.; Opsteegh, J.D.; van Oldenborgh, G.J.; Burgers, G. Estimating return periods of extreme events from ECMWF seasonal forecast ensembles. *Int. J. Climatol.* **2005**, *25*, 1345–1354. [[CrossRef](#)]
78. Jacobeit, J.; Wanner, H.; Luterbacher, J.; Beck, C.; Philipp, A.; Sturm, K. Atmospheric circulation variability in the North-Atlantic-European area since the mid-seventeenth century. *Clim. Dyn.* **2003**, *20*, 341–352. [[CrossRef](#)]
79. Nied, M.; Pardowitz, T.; Nissen, K.; Ulbrich, U.; Hundecha, Y.; Merz, B. On the relationship between hydro-meteorological patterns and flood types. *J. Hydrol.* **2014**, *519*, 3249–3262. [[CrossRef](#)]
80. Merz, B.; Aerts, J.; Arnbjerg-Nielsen, K.; Baldi, M.; Becker, A.; Bichet, A.; Blöschl, G.; Bouwer, L.M.; Brauer, A.; Cioffi, F.; et al. Floods and climate: Emerging perspectives for flood risk assessment and management. *Nat. Hazards Earth Syst. Sci.* **2014**, *14*, 1921–1942. [[CrossRef](#)]
81. Christensen, J.H.; Boberg, F.; Christensen, O.B.; Lucas-Picher, P. On the need for bias correction of regional climate change projections of temperature and precipitation. *Geophys. Res. Lett.* **2008**, *35*. [[CrossRef](#)]
82. Ehret, U.; Zehe, E.; Wulfmeyer, V.; Warrach-Sagi, K.; Liebert, J. HESS Opinions “should we apply bias correction to global and regional climate model data?”. *Hydrol. Earth Syst. Sci.* **2012**, *16*, 3391–3404. [[CrossRef](#)]
83. Sippel, S.; Otto, F.E.L.; Forkel, M.; Allen, M.R.; Guillod, B.P.; Heimann, M.; Reichstein, M.; Seneviratne, S.I.; Thonicke, K.; Mahecha, M.D. A novel bias correction methodology for climate impact simulations. *Earth Syst. Dyn.* **2016**, *7*, 71–88. [[CrossRef](#)]

84. Hattermann, F.F.; Krysanova, V.; Gosling, S.N. Cross-scale intercomparison of climate change impacts simulated by regional and global hydrological models in eleven large river basins. *Clim. Chang.* **2017**, *141*, 561–576. [[CrossRef](#)]
85. Zhao, F.; Masaki, Y.; Hanasaki, N.; Biemans, H.; Zaherpour, J.; Gosling, S.N.; Veldkamp, T.I.E.; Frieler, K.; Schewe, J.; Ostberg, S.; et al. The critical role of the routing scheme in simulating peak river discharge in global hydrological models The critical role of the routing scheme in simulating peak river discharge in global hydrological models. *Environ. Res. Lett.* **2017**, *12*, 075003. [[CrossRef](#)]
86. Zaherpour, J.; Masaki, Y.; Hanasaki, N.; Gosling, S.N.; Mount, N.; Hannes, M.; Ted, I.E. Worldwide evaluation of mean and extreme runoff from six global-scale hydrological models that account for human impacts OPEN ACCESS Worldwide evaluation of mean and extreme runoff from six global-scale hydrological models that account for human impacts. *Environ. Res. Lett.* **2018**, *13*, 065015. [[CrossRef](#)]
87. Adam, L.; Eisner, S.; Reinecke, R.; Riedel, C.; Döll, P.; Song, Q.; Müller Schmied, H.; Fink, G.; Zhang, J.; Portmann, F.T.; et al. Variations of global and continental water balance components as impacted by climate forcing uncertainty and human water use. *Hydrol. Earth Syst. Sci.* **2016**, *20*, 2877–2898.
88. Franz, D.; Portmann, F.T.; Döll, P.; Eisner, S.; Flörke, M.; Wattenbach, M.; Müller Schmied, H. Sensitivity of simulated global-scale freshwater fluxes and storages to input data, hydrological model structure, human water use and calibration. *Hydrol. Earth Syst. Sci.* **2014**, *18*, 3511–3538.
89. Heinke, J.; Gudmundsson, L.; Voss, F.; Koirala, S.; Clark, D.B.; Hagemann, S.; Hanasaki, N.; Gerten, D.; Tallaksen, L.M.; Stahl, K.; et al. Comparing Large-Scale Hydrological Model Simulations to Observed Runoff Percentiles in Europe. *J. Hydrometeorol.* **2011**, *13*, 604–620.
90. Wiltshire, A.J.; Ludwig, F.; Chen, C.; Clark, D.B.; Voss, F.; Hanasaki, N.; Gosling, S.N.; Haddeland, I.; Hagemann, S.; Heinke, J.; et al. Climate change impact on available water resources obtained using multiple global climate and hydrology models. *Earth Syst. Dyn.* **2013**, *4*, 129–144.
91. Lo, M.H.; Famiglietti, J.S. Effect of water table dynamics on land surface hydrologic memory. *J. Geophys. Res. Atmos.* **2010**, *115*, 1–12. [[CrossRef](#)]
92. Middelkoop, H.; Daamen, K.; Gellens, D.; Grabs, W.; Kwadijk, J.C.J.; Lang, H.; Parmet, B.W.A.H.; Schädler, B.; Schulla, J.; Wilke, K. Impact of Climate Change on Hydrological Regimes and Water Resources Management in the Rhine Basin. *Clim. Chang.* **2001**, *49*, 105–128. [[CrossRef](#)]



© 2019 by the authors. Licensee MDPI, Basel, Switzerland. This article is an open access article distributed under the terms and conditions of the Creative Commons Attribution (CC BY) license (<http://creativecommons.org/licenses/by/4.0/>).